Theory of melting at high pressures: Amending density functional theory with quantum Monte Carlo

L. Shulenburger, M. P. Desjarlais, and T. R. Mattsson

Theory of melting at high pressures: Amending Density Functional Theory with Quantum Monte Carlo

L. Shulenburger,[*] M. P. Desjarlais,[†] and T. R. Mattsson[‡]

Sandia National Laboratories, Albuquerque, New Mexico 87185, USA

(Dated: September 30, 2014)

We present an improved first-principles description of melting under pressure based on thermodynamic integration comparing Density Functional Theory (DFT) and quantum Monte Carlo (QMC) treatments. The method is applied to address the longstanding discrepancy between density functional theory (DFT) calculations and diamond anvil cell (DAC) experiments on the melting curve of xenon, a noble gas solid where van der Waals binding is challenging for traditional DFT methods. The calculations show agreement with data below 20 GPa and that the high-pressure melt curve is well described by a Lindemann behavior up to at least 80 GPa in contrast to DAC data.

The high pressure melt line of simple materials carries great significance in both theoretical and in practical applications. For instance, the rapid decrease followed by suspected increase in the melting temperature of lithium under pressure is a bellwether for the complex series of solid phases that exist at lower temperatures.[1] Furthermore, the onset of melt triggers a dramatic loss of mechanical strength of a material, with significant changes in dynamic behavior following. In fact, the point where a material melts under shock compression is one of the key properties that can distinguish between possible scenarios for planetary accretion.[2] Although diamond anvil cell (DAC) experiments remain the most versatile experimental technique for probing high pressure melting behavior, they have also been a source of controversy. Important examples exist in the literature of melt lines showing an anomalous change in slope under pressure that were contradicted by either shock experiments or later DAC experiments.[3,4] An as yet unchallenged melt line of this type is exhibited by xenon and other noble gases - which are of particular importance due to their inert nature. The high pressure behavior of the noble gases is a fundamental test of the DAC methodology and as such deserves special scrutiny. Specifically, we consider the behavior of xenon and find that the high-pressure melting behavior is well described by a traditional melting curve.

As alluded to above, the experimentally obtained melting curve for xenon exhibits an interesting feature when probed in the diamond anvil cell, abruptly flattening at pressures above 25 GPa.[5] This observation prompted much theoretical attention, including the application of quantum mechanical simulation techniques.[6] These techniques, lead by density functional theory (DFT), are uniquely suited to the study of extreme conditions as their fundamental approximations are not affected by the presence of temperature or pressure. If a calculation is accurate near ambient conditions, the method is also likely to be accurate at high pressure. DFT applied to xenon supports a Lindemann melt curve in contrast to experiments.[6]

The accuracy of DFT calculations of noble gases, however, is not to be taken for granted since fundamental uncertainties remain regarding calculations of systems where van der Waals interactions are significant. Standard semi-local functionals such as the local density approximation (LDA) tend to over-bind the noble gases due to a self interaction of the electrons in regions of low density. Second generation GGA functionals such as AM05[7] remove this self-interaction, but as a result do not bind noble gas solids at all. Despite much progress in the area of dispersion corrected DFT,[8] cases where dispersion dominated bonding gives way to covalent-or metallic bonding remain a challenge. Xenon presents a canonical example of this effect and as a result its behavior is greatly affected by pressure. Xenon turns metallic under moderate shock compression[9] and although xenon is a narrow-range cryogenic liquid at normal pressure with melting and boiling points of 161.4 K and 165.0 K, respectively, at 20 GPa the melting point is above 2500 K.

These significant theoretical challenges necessitate the application of a complementary technique whose approximations are not tied to the local behavior of the electrons. A promising candidate from this point of view is diffusion quantum Monte Carlo (DMC).[10,11] Whereas the approximation made in DFT calculations requires the consideration of an effective Hamiltonian, DMC treats the Hamiltonian exactly. Therefore, DMC can accurately study van der Waals interactions and has been successfully applied to noble gas solids[12,13] and the interactions between filled shell molecules.[14–17]

In order to thoroughly investigate the performance of DMC for xenon, we focused on the three fundamental approximations in the calculations. These approximations are the pseudopotential approximation that is necessary for computational efficiency, the fixed node approximation which is necessary to mitigate the fermion sign problem, and the finite size approximation where calculations on modest sized supercells are used to determine properties xenon in the thermodynamic limit.

As a test of these approximations, the energy versus volume for the FCC crystal is used as a benchmark. Calculations of a 32 atom supercell, using the finite size correction methods employed in the rest of the paper with two different starting points are considered. Firstly pseu-
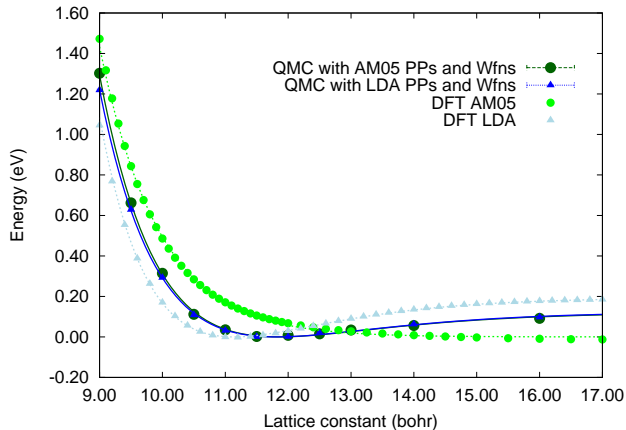
FIG. 1. (color online) Energy of a unit cell of FCC xenon calculated with DFT and DMC. The dotted lines correspond to Vinet fits to the DFT calculations. The solid lines correspond to Vinet fits to the DMC calculations. The triangles correspond to DFT or DMC simulations based on the LDA and the circles DFT or DMC based on AM05.

dopotentials and nodal surfaces from the LDA are used as input to the DMC calculations. Then the processes is repeated with pseudopotentials and nodal surfaces from AM05, allowing a sensitivity test to the form of these approximations. The results of this test are shown in Fig 1. We find that the DMC results are independent of the trial wavefunctions and pseudopotentials to the level required for this work. Fitting the DMC energy versus volume curve with a Vinet form[18] gives a lattice constant varying by only $0.25\% \pm 0.61\%$ when changing from LDA to AM05 trial wavefunctions and a bulk modulus varying by only $0.4\% \pm 0.8\%$. For this reason we conclude the errors arising from nodal and pseudopotential approximations are small for these DMC calculations of xenon.

Despite this evidence that DMC is ideally suited for the calculation of the properties of xenon under pressure, an important wrinkle remains. Direct calculations of melting are not currently feasible with DMC for anything beyond the lightest of elements. Fortunately, a solution to this problem has recently been proposed: thermodynamic integration can be used to connect the accuracy of the DMC calculations with the speed and efficiency of DFT based molecular dynamics.[19] Using this technique, Sola and Alfé found that DMC calculations favored the solid phase in calculations of the melting of iron under pressure. This result was in disagreement with DAC experiments.[20] A potential concern with this result is that QMC methods (both VMC and DMC) being variational tend to produce relatively lower total energies for more ordered states (in this case solids versus liquids). This effect is because the trial wavefunctions used tend to be rather simple compared to the true many body wavefunctions and typically do not increase in complexity for the less ordered phases. Thus simpler phases where the wavefunction is closer to the many body wavefunction tend to have a smaller positive fixed node error than

more complex phases.

In light of this and because the approach is new, we elected to null-test the method by calculating the melting temperature of aluminum at 120 GPa. This material and condition were chosen because shock experiments, diamond anvil cell experiments and DFT calculations all agree as to the melting temperature.[21] If the QMC free energies were biased towards the solid phase then the melting temperature would be overestimated using this method. Relative energies between the snapshots of the same phase for aluminum agreed very well between the DMC and DFT, giving confidence that the DFT dynamics were close to the DMC ones. Additionally, the shift in free energy between the solid and liquid was very small, 0.202 ± 0.100 meV/atom, leading to a temperature shift of only 2.3 ± 1.2 K. This result is well within the errors of the method and experimental accuracy for melting under pressure. Furthermore, this test shows that the thermodynamic integration method does not suffer from notable systematic errors when the DMC is performed with a relatively simple trial wavefunction.

In applying this approach to the melting of xenon we start by calculating the melting line at two points using DFT based molecular dynamics. Specifically following the work of Root et al.[22] we performed calculations using VASP[23] within the AM05[7] density functional. These calculations started with FCC solid in the same simulation cell as liquid xenon. Care was taken to ensure that nonhydrostatic stresses were minimized via an equilibration procedure taking over 1000 two femtosecond time steps and 220 eV plane wave cutoffs. Two densities were selected for these simulations, 7.27 g/cc and 10.0 g/cc. As the finite size of the simulation cell is a concern with this type of calculation we performed two different procedures, one in the NVT ensemble that brackets the melt line by performing calculations at different temperatures and looking at whether the cell has frozen or melted after a period of ≈ 8 ps, and another one in the NVE ensemble that establishes a coexistence between the two phases and measures the temperature of the resulting assembly again over ≈ 8 ps, which allows the temperature to be determined to within ≈ 20 K for the larger simulation cells. We found that for the higher density, calculations with 214 xenon atoms found a melt temperature of 6000 K in the NVT ensemble, but NVE yielded a lower value. This suggested that larger simulation cells were necessary and cells doubled in size in the direction perpendicular to the interface (428 atoms) found agreement, yielding two points at which the Gibbs free energy of the two phases were equal: 24.4 GPa and 3000 K for 7.27 g/cc and 74.4 GPa and 5600 K for 10.0 g/cc.

From this foundation, we followed Sola and Alfé[19] adding refinements to the methodology. The change in free energy of a phase at a given temperature and volume is calculated by taking snapshots from long DFT based molecular dynamics simulations and comparing the energy of those snapshots to energies from DMC calculations. Using this information, the change in the

Helmholtz free energy of each phase is found using a perturbation series of cumulants in the energy difference as:

$$\Delta F = \sum_{n=0}^{\infty} \frac{(1/k_B T)^{n-1}}{n!} \kappa_n \tag{1}$$

where the κ_n's are cumulants of the difference in internal energy between the DMC and DFT ensembles:

$$\kappa_0 = \langle \Delta U \rangle_{\lambda=0}$$
$$\kappa_1 = \langle \Delta U^2 \rangle_{\lambda=0} - \langle \Delta U \rangle_{\lambda=0}^2$$
$$\vdots \tag{2}$$

or directly in terms of the partition function

$$\Delta F = -k_B T \left\langle e^{-\Delta U/k_B T} \right\rangle_{\lambda=0} \tag{3}$$

where $\Delta U = U_{DMC} - U_{DFT}$ with U_{DMC} and U_{DFT} the potential energies of the DMC and DFT systems respectively and $\langle \rangle_\lambda$ represents the thermal average in the ensemble generated by the potential energy function $U(\lambda) = \lambda U_{DMC} + (1-\lambda)U_{DFT}$. The approximation above is valid when U_{DMC} and U_{DFT} are sufficiently close so that the averages over all of state space can be approximated using a few configurations sampled from the ensemble of the reference system. A necessary condition for this to be valid is that the higher order terms in Eq. 1 are small and that the two approximations in Eq. 1 and Eq. 3 yield very similar answers. A test of this condition is found in Fig. 2. From this figure, it is apparent that the total energies track each other well, again suggesting that DFT provides a faithful sampling of the energy landscape. Quantitatively, Eq. 1 bears this out, with the second term in the cumulant expansion being 1.5% of the first one for the solid at 7.27 g/cc and 1.4% for the liquid. The bottom panel in Fig. 2 shows the differences between the solid and the liquid snapshots after the average DMC-DFT energy difference for the solid is subtracted for all points. This shows visually that the DMC energy is on average 35.0 meV/atom larger for the liquid snapshots than the corresponding DFT.

Given that the change in Helmholtz free energy at constant volume can be calculated for the solid and liquid, how should this knowledge be used to calculate a change in melt temperature or pressure? The start of such methods is the equality of the Gibbs free energy between the solid and liquid. Following the work of Sola and Alfe,[19] for a given density and temperature, the change in the Gibbs free energy for a phase when moving from DFT interactions to QMC is

$$\Delta G \approx \Delta F - V \Delta p^2 / 2B_T \tag{4}$$

with B_T the isothermal bulk modulus and Δp the change in pressure as the potential energy is changed from U_{DFT} to U_{DMC} at constant volume. In previous work on iron,[19] it was argued that the second term on the right hand
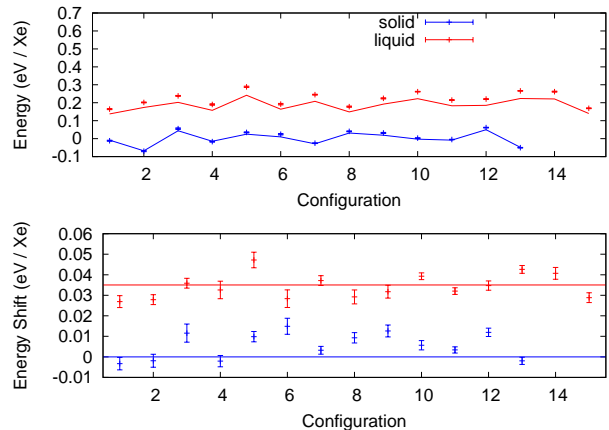

FIG. 2. (color online) Top: DMC energies corresponding to configurations representative of solid (blue triangles) and liquid (red squares) xenon, generated with QMD on 108 atom systems. The solid lines connect DFT energies calculated on the same configurations. An independent offset is added to the DMC and DFT calculations so that the average energy of the solid snapshots in each method is 0. Bottom: DMC-DFT energy differences for the same configurations. The average DMC-DFT energy difference for the solid is subtracted from all points. Lines represent the average of the energy differences between DMC and DFT in the solid and the liquid.

side of the equation is small and only the change of free energy was used. Given the deficiencies of semilocal DFT in treating xenon, we evaluate these directly.

In order to evaluate the isothermal bulk modulus and the change in pressure, we used thermodynamic integration to construct the relative Helmholtz free energies within each phase using QMD. This was done by calculating the average pressure in QMD calculations for several densities along an isotherm and constructing relative free energies using the following expression:

$$dF = -\int_{V_i}^{V_f} P dV + C. \tag{5}$$

Next, we use the calculated melting pressure at this temperature to determine the relative free energy between the solid and liquid. The first thing this procedure allows is for the specific volumes at which the solid and liquid coexist to be determined. These are the volumes at which the change in free energy referenced by Eq. 4 should be calculated. Next, we calculate the shift in the Helmholtz free energy when changing from DFT to DMC for each phase at three different volumes along these isotherms. This procedure allows the volume dependent Helmholtz free energy within the DMC ensemble to be determined for each phase.

Having constructed the relative free energies of the solid and liquid with a DFT determined interaction and a DMC determined one, we determine the change in the melting conditions in two ways. The first is to use the Gibbs construction to determine the melting pressure in
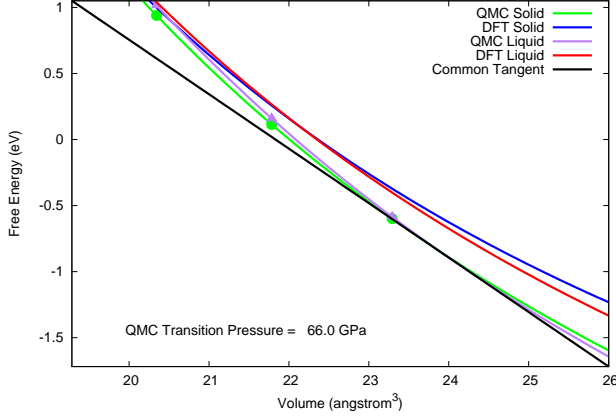
FIG. 3. (color online) Relative Helmholtz free energy of the solid and liquid phases at 5600K determined by DFT calculations to establish the melt pressure and thermodynamic integration to find the relative free energies. A common tangent to the QMC curves is also shown, establishing a new melt pressure of 66 GPa.

the DFT ensemble as illustrated in Fig.3. This yields a shift in the melting pressure at 3000K from 24.4 GPa to 23.4 GPa and at 5600K from 74.4 GPa to 66.0 GPa. Alternatively, we can calculate the shift in the Gibbs free energy at the density of coexistence in each phase. The change in temperature necessary to restore the equality of the Gibbs free energy is:

$$\Delta T^m \simeq G^{ls}/S^{ls}_{DFT} \tag{6}$$

This procedure shifts the melting temperature at 24.4 GPa from 3000K to 3155K and at 74.4 GPa from 5600K to 5810K.

It is particularly instructive to note what would have happened if we had assumed that the shift to the free energy as a function of volume was constant as was argued for iron in Ref. 19. With this simplifying assumption, it is no longer necessary to determine the correction to the free energy at the specific volumes of the coexistence, rather it can be done at a convenient density (the density where the Helmholtz free energy of the two phases is equal is a typical choice). This however, proves to be a poor assumption for high pressure xenon, with considerably larger shifts to the melting temperature (at 24.4 GPa, the temperature shifts is 315K instead of 155K and at 74.4 GPa is 530K instead of 210K). Similarly, the Gibbs construction can be used to calculate the change to the melting pressure but now with the DFT values being shifted by a volume independent constant. Again, this results in a much larger shift to the pressure, going from 24.4 GPa at 3000K to 17.7 GPa and from 74.4 GPa at 5600K to 51.7 GPa.

Our results for the high pressure melting of xenon are summarized in Fig. 4. Our DFT calculated values are shown as green triangles which agree well with earlier values calculated by Belonohsko et al.[26] The values from
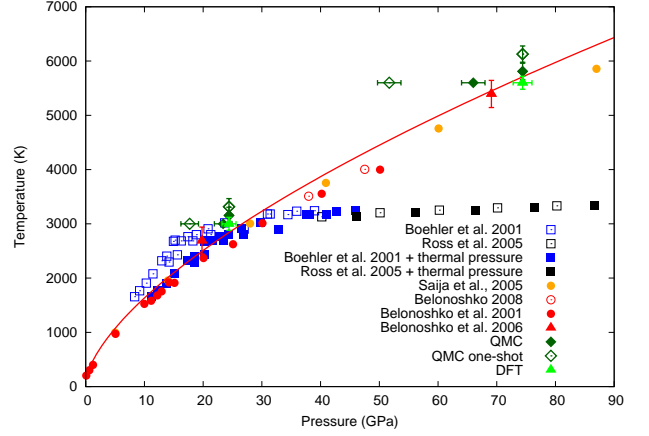

FIG. 4. (color online) Melting of xenon as a function of pressure obtained with various theoretical[6,24–26] and experimental[5,27] techniques. Experimental points are solid squares, classical molecular dynamics circles, DFT based molecular dynamics triangles and QMC diamonds. A correction of the experimental points including an estimate of thermal pressure from SESAME 5191[28] is shown with filled pentagons. Horizontal error bars on the QMC points include the statistical uncertainty in the pressure shift technique, the vertical error bars from the temperature shift technique.

using the thermodynamic integration to DMC are shown as closed diamonds with open diamonds the values from assuming that the shift is constant as a function of volume. The net effect of these corrections is to increase the disagreement between the melting at high pressure and the DAC experiments. At lower pressures, our results appear to be in slightly better agreement with the DAC experiments. However, it should be noted that the DAC experiments likely are not isobaric during the heating as their pressure measurements would imply. If we instead assume that they are isochoric, we can calculate the thermal pressure at the melting temperature for each density using an equation of state,[28] resulting in corrected pressures as shown in Fig. 4. These results for xenon suggest that the high pressure DAC experiments should be reexamined to rule out either surface effects, non-hydrostatic stresses, or melting from a different phase as the cause of the reported flat melting line.[29] This result might be achieved by exploiting a bulk probe of the xenon structure such as x-ray diffraction rather than the speckle field technique that was previously used.[5]

We have presented an extension of the methodology of using thermodynamic integration to determine melting conditions, improving the accuracy for compressible materials and showing that considering the volume dependence of the free energy shift is crucial. This high-accuracy procedure can be used to further explore the melting behavior of a wide variety of materials, thereby contributing to the ability of hydrodynamic simulations to predictively model a wide range of phenomena from inertial confinement fusion to planetary science.

The authors acknowledge helpful discussions with Ken

* lshulen@sandia.gov

† mpdesja@sandia.gov

‡ trmatts@sandia.gov

[1] C. L. Guillaume, E. Gregoryanz, O. Degtyareva, M. I. McMahon, M. Hanfland, S. Evans, M. Guthrie, S. V. Sinogeikin, and H. Mao, Nature Physics **7**, 211 (2011).

[2] T. W. Dahl and D. J. Stevenson, Earth and Planetary Science Letters **295**, 177 (2010).

[3] A. Dewaele, M. Mezouar, N. Guignot, and P. Loubeyre, Phys. Rev. Lett. **104**, 255701 (2010).

[4] S. Anzellini, A. Dewaele, M. Mezouar, P. Loubeyre, and G. Morard, Science **340**, 464 (2013).

[5] M. Ross, R. Boehler, and P. Soderlind, Phys. Rev. Lett. **95**, 257801 (2005).

[6] A. B. Belonoshko, S. Davis, A. Rosengren, R. Ahuja, B. Johansson, S. I. Simak, L. Burakovsky, and D. L. Preston, Phys. Rev. B **74**, 054114 (2006).

[7] R. Armiento and A. E. Mattsson, Phys. Rev. B **72**, 085108 (2005).

[8] Y. Andersson, D. C. Langreth, and B. I. Lundqvist, Phys. Rev. Lett. **76**, 102 (1996).

[9] W. J. Nellis, M. van Thiel, and A. C. Mitchell, Phys. Rev. Lett. **48**, 816 (1982).

[10] W. M. C. Foulkes, L. Mitas, R. J. Needs, and G. Rajagopal, Rev. Mod. Phys. **73**, 33 (2001).

[11] L. Shulenburger and T. R. Mattsson, Phys. Rev. B **88**, 245117 (2013).

[12] N. D. Drummond and R. J. Needs, Phys. Rev. B **73**, 024107 (2006).

[13] A. Benali, L. Shulenburger, N. A. Romero, J. Kim, and O. A. von Lilienfeld, Journal of Chemical Theory and Computation **10**, 3417 (2014).

[14] S. Sorella, M. Casula, and D. Rocca, Journal of Chemical Physics **127**, 014105 (2007).

[15] T. D. Beaudet, M. Casula, J. Kim, S. Sorella, and R. M. Martin, Journal of Chemical Physics **129**, 164711 (2008).

[16] M. Dubecký, P. Jurecka, R. Derian, P. Hobza, M. Otyepka, and L. Mitas, Journal of Chemical Theory and Computation **9**, 4287 (2013).

[17] M. Dubeckỳ, R. Derian, P. Jurečka, L. Mitas, P. Hobza, and M. Otyepka, Physical Chemistry Chemical Physics **16**, 20915 (2014).

[18] P. Vinet, J. Ferrante, J. R. Smith, and J. H. Rose, Journal of Physics C: Solid State Physics **19**, L467 (1986).

[19] E. Sola and D. Alfè, Phys. Rev. Lett. **103**, 078501 (2009).

[20] R. Boehler, Nature **363**, 534 (1993).

[21] J. Bouchet, F. Bottin, G. Jomard, and G. Zérah, Phys. Rev. B **80**, 094102 (2009).

[22] S. Root, R. J. Magyar, J. H. Carpenter, D. L. Hanson, and T. R. Mattsson, Phys. Rev. Lett. **105**, 085501 (2010).

[23] G. Kresse and J. Furthmuller, Phys. Rev. B **54**, 11169 (1996).

[24] F. Saija and S. Prestipino, Phys. Rev. B **72**, 024113 (2005).

[25] A. B. Belonoshko, R. Ahuja, and B. Johansson, Phys. Rev. Lett. **87**, 165505 (2001).

[26] A. B. Belonoshko, Phys. Rev. B **78**, 174109 (2008).

[27] R. Boehler, M. Ross, P. Söderlind, and D. B. Boercker, Phys. Rev. Lett. **86**, 5731 (2001).

[28] J. Carpenter, D. Flicker, S. Root, R. Magyar, D. Hanson, and T. Mattsson, EPJ Web of Conferences **10**, 00018 (2010).

[29] A. B. Belonoshko and L. S. Dubrovinsky, American Mineralogist **82**, 441 (1997).